Effect of silica colloids on the rheology of viscoelastic gels formed by the surfactant cetyl trimethylammonium tosylate

Ranjini Bandyopadhyay [1] **and A. K. Sood**

Department of Physics, Indian Institute of Science, Bangalore 560 012, India

Abstract

The effects of the addition of sub-micrometer sized colloidal silica spheres on the linear and nonlinear rheology of semi-dilute solutions of a viscoelastic gel are studied. For a 1.4 wt.% solution of the surfactant CTAT, a peak in the zero shear rate viscosity $\eta_\circ$ is observed at approximately equal weight percents of silica and CTAT. This peak shifts to lower silica concentrations on increasing either the CTAT concentration or the surface charge on silica and disappears when the CTAT concentration is increased to 2.6wt%. The increases in $\eta_\circ$ and the high frequency plateau modulus $G_\circ$ on the introduction of SiO_2 are explained by considering the increasingly entangled wormlike micelles that are formed due to the enhanced screening of the electrostatic interactions. The observed decrease in the values of $G_\circ$ and $\eta_\circ$ at higher concentrations of silica particles is explained in terms of the formation of surfactant bilayers due to the adsorption of the positively charged cetyl trimethylammonium to the negatively

[1] presently at the Department of Physics and Astronomy, Johns Hopkins University, Baltimore MD 21218, USA, Email: ranjini@pha.jhu.edu

charged silica.

1 Introduction

The study of the rheology of surfactants, polymers, polyelectrolytes and their composites is interesting, not only from an academic point of view, but also in the context of possible industrial applications. Viscoelastic surfactant solutions are ideal candidates for the study of complex flow phenomena [1], while mixtures of colloids and liquid crystals form novel composite materials under certain conditions. There has been extensive work on the dramatic changes in the rheology of liquid crystals on the addition of colloidal particles [2, 3, 4]. When latex microspheres bind to flexible giant vesicles, the resulting membrane distortions induce interparticle attractions and the subsequent formation of close-packed and ring-like particle aggregates [5]. Recent x-ray studies show that mixtures of DNA and cationic or neutral liposomes form stacks of two-dimensional smectics of aligned DNA chains intercalated by lipid bilayers [6]. The experiments of Solomon *et al.* [7] prove that the yielding of concentrated zirconia suspensions is extremely sensitive to the headgroup chemical structure of the added surfactant. Phase separations in a mixture of hard-sphere rods and colloids have been observed experimentally, where spontaneous demixing into rod-rich and rod-poor states, alternating layers of rods and spheres, columns of spheres in a crystalline array etc. are seen to occur [8]. Recent experiments have shown a variety of structures (2D hexagonal, lamellar and 2D centered rectangular phase) formed

by complexation of cationic and anionic surfactant mixtures with polyelecrolytes like DNA, poly-glutonic acid, poly-acrylic acid and polystyrene sulfonate [9].

In addition to the systems mentioned above, extensive experimental investigations have been cconducted on mixtures of different species of surfactants and polymers. Cetyl trimethylammonium bromide (CTAB) micelles show a dramatic increase in length when mixed with a few molecules of oppositely-charged gemini surfactants [10]. The results are explained in terms of the cross-linking of the CTAB micelles by the gemini surfactants. Viscometric measurements on mixtures of cetyl trimethylammonium tosylate (CTAT) and cetyl trimethylammonium 3-hydroxy naphthalene 2- carboxylate (CTAHNC) show a peak in the zero-shear viscosity $\eta_\circ$ with increasing HNC^- concentration [11]. The added HNC^- is thought to increase the micellar hydrophobicity, which encourages micellar growth and increases the solution viscosity. The subsequent decrease in $\eta_\circ$ is understood in terms of the formation of intermicellar connections. Addition of the anionic micelle sodium dodecyl sulphate (SDS) to hydrophobically modified poly(sodium acrylate) (HMPAA) also shows a peak in the viscosity [12]. A maximum in the viscosity of the polymer poly(ethyleneoxide) (PEO) on the addition the surfactant SDS is explained in terms of a polymer-surfactant complex formation [13]. This peak is shown to correspond to the concentration of SDS at which the polymer coils get saturated with the added surfactant. Addition of methyl-Na-benzoates to cetyl pyridinium chloride (CPyCl) results in a peak in the zero-shear viscosity [1]. This is explained in terms of

a rapid, micellar growth followed by cross-linking of the micelles in the presence of the hydrophobic methyl-Na-benzoate. The stress relaxation changes from multi-exponential to mono-exponential across the viscosity peak, indicating a cross-over from diffusion-controlled to kinetically-controlled processes. It is thus easy to control the rheology of polymer and surfactant solutions by changing the counterion concentration or by introducing micron-sized colloidal additives. Addition of hydrophobic counterions or colloidal particles modifies the inter-micellar interactions and alters the micellar packing considerations, and in some cases, may even result in phase transitions and the formation of novel complexes.

In this paper, we discuss our work on the rheology of semi-dilute solutions of wormlike micelles (cetyl trimethylammonium tosylate) in the presence of submicrometer sized particulate additives (monodisperse silica colloids of diameter 0.1 μm). In addition to the frequency dependent elastic modulus $G'(\omega)$ and the loss modulus $G''(\omega)$, we measure the shear rate dependent viscosity $\eta(\dot{\gamma})$ of the samples, and by fitting these to appropriate models, extract the relaxation times τ_R, the zero shear viscosities $\eta_\circ$ and the high frequency plateau moduli $G_\circ$ of the mixtures as a function of the weight percent of added silica (SiO_2) particles. We explain our observations by considering the changes in inter-macromolecular interactions that arise out of the presence of colloidal additives in the viscoelastic gel.

2 Experimental

CTAT powder, purchased from Sigma Chemicals, Bangalore, India, is weighed carefully and dissolved at weight percents of 1.4wt.% (31mM), 1.95wt.% (43mM) and 2.6wt.% (53mM) in aqueous colloidal silica suspensions prepared at weight percents 0.85wt.%, 1.05wt.%, 1.4wt.%, 1.95wt.%, 2.6wt.%, 3.9wt.% and 5.2wt.%. The silica colloids were obtained as a gift from Nissan Chemicals, Japan. Pure samples of CTAT are also prepared at weight percents 1.4 wt.%, 1.95 wt.% and 2.6 wt.% to understand the role of the colloidal silica on the rheology of the viscoelastic gel phase of CTAT. In this concentration range, the zero shear viscosity $\eta_\circ$ of CTAT is found to vary with CTAT concentration c as $\eta_\circ \sim c^{3.8}$. The CTAT - silica mixtures are allowed to equilibrate at 30°C for a week. The silica suspensions in which CTAT is dissolved are prepared from a stock solution of monodisperse colloidal silica (diameter = 0.1 μm, density = 1.29 g/cc. and weight fraction 39.3%), diluted with deionized and distilled water to the required concentrations. The effect of electrostatic interactions on micellar aggregation in the presence of colloidal SiO_2 is studied by increasing the surface charge on the SiO_2 particles. This is achieved by adding minute quantities of sodium hydroxide ([NaOH] $\sim$ 0.178mM) to the silica suspensions. Addition of NaOH to SiO_2 results in the increased dissociation of the surface silanol groups, which leads to an increase in the surface charge density of the silica particles [14].

All the rheological measurements are performed in a cone-and-plate geometry (cone angle = $1°59'$, diameter = 4 cm) in an AR-1000N Rheolyst stress-

controlled rheometer (T. A. Instruments, U.K). The sample temperature is controlled at 25°C for all the experiments. Direct visualization of the samples under ambient conditions using optical microscopy shows no evidence of phase separation.

3 Linear rheology

In viscoelastic gel-forming surfactant solutions, the stress relaxation is governed by the breaking and reformation time τ_{break} and the reptation or curvilinear diffusion time τ_{rep} of the micelles. In the limit where $\tau_{break} << \tau_{rep}$, the resulting single exponential stress relaxation can be fit to the Maxwell model, where the characteristic relaxation time $\tau_R = \sqrt{\tau_{rep}\tau_{break}}$. Fig. 1 shows the frequency response data for CTAT 1.4wt.% samples, with (a) 0wt.%, (b) 1.3wt.% and (c) 5.2wt.% silica. The elastic modulus $G'(\omega)$ and the viscous modulus $G''(\omega)$ do not show pure Maxwellian behavior, and are fit to the Cole-Davidson model [15] which predicts a stretched exponential form for the stress relaxation and works well for many glass-forming liquids. In this model, the dynamic modulus is expressed as $G^{\star}(\omega) = G_{\circ}[1 - \frac{1}{(1+i\omega\tau_R)^{\alpha}}]$, where $G_{\circ}$ is the high frequency plateau modulus and τ_R is a measure of an average relaxation time. The inverse of the exponent α characterizes the width of the relaxation spectrum and equals 1 for Maxwellian relaxation [16, 17]. A decrease in α from its maximum value of 1 indicates the presence of multiple stress relaxation processes. The frequency dependent moduli measured in our experiments are fit to the Cole-Davidson

model with $G_\circ$, τ_R and α as the fitting parameters. For angular frequencies $\omega < 2$ rad/sec, the fits (shown as solid lines in fig. 1) are found to improve as the concentration of silica additives in the CTAT solutions is increased. The deviations observed at high angular frequencies ($\omega > 2$ rad/sec) can be attributed to the effects of breathing (axial stretching modes arising from tube length fluctuations) and Rouse modes [18, 19] on the stress relaxation processes in the samples. Fig. 2 shows the plot of the fitted values of α as a function of increasing SiO_2 content. The values of α, also tabulated in table 1, are found to increase monotonically with SiO_2 concentration, implying a separation in the relaxation time scales and a tendency towards increasingly mono-exponential relaxation on the addition of SiO_2 particles. τ_R may also be calculated from the crossover frequency ω_{co} at which $G'(\omega)$ and $G''(\omega)$ are equal, by using the relation $\tau_R = \omega_{co}^{-1}$. A good indication of single exponential stress relaxation is the semi-circular form of the so-called Cole-Cole figure, where the viscous modulus normalized by the high frequency shear modulus $G_\circ$ is plotted *vs.* the normalized elastic modulus. Fig. 3 shows the Cole-Cole plot corresponding to the data plotted in Fig. 1. The plot for the sample with 5.2 wt.% SiO_2 in CTAT approaches the semi-circular form indicative of the dominance of a unique stress relaxation mechanism. The Cole-Cole plot for the pure 1.4 wt.% CTAT is almost linear and implies a distribution of relaxation time scales, possibly arising out of competing processes (for example, comparable breakage and reptation times). Figs. 4 (a), (b) and (c) show the plots of the dynamic viscosity $\eta^\star$ normalized

by the zero-shear viscosity $\eta_\circ$ (open squares) for the same three samples, where $\eta^\star(\omega) = \frac{\sqrt{G'^2+G''^2}}{\omega}$. The dashed lines show the fits to the model for giant wormlike micelles given by $\eta^\star(\omega) = \frac{\eta_\circ}{\sqrt{1+\omega^2\tau_R^2}}$ [20], where τ_R is the average relaxation time discussed earlier. The fits of $\eta^\star(\omega)$ to this model are found to work best at intermediate SiO_2 concentrations. These results can be interpreted in terms of the growth of entangled wormlike micelles, followed by the formation of bilayers due to the adsorption of the headgroups on the SiO_2 surfaces.

4 Nonlinear rheology

The zero-shear viscosities $\eta_\circ$ of all the samples are also calculated by fitting the shear-viscosity ($\eta(\dot\gamma)$) *vs.* shear rate ($\dot\gamma$) data obtained in the flow experiments to the Giesekus model [21]. The Giesekus model considers the orientation effects of flow by introducing a deformation dependent tensorial mobility of breaking and reforming micelles and predicts the shear-rate dependent viscosity $\eta(\dot\gamma) = \frac{\eta_\circ}{2\tau_R\dot\gamma^2}[\sqrt{1+4\tau_R\dot\gamma^2}-1]$. This expression is an analytical solution of a constitutive equation for the viscoelastic properties of entangled micelles and assumes an adjustable parameter $\alpha' = 0.5$ [1], where α' is a dimensionless anisotropy factor which is related to the relative mobility tensor β and the configuration tensor C by the relation $\beta = 1+\alpha(C-1)$. We would like to note here that experimental data for wormlike micellar solutions usually satisfy $\alpha' = 0.5$ [1]. In addition to plots of $\eta^\star(\omega)/\eta_\circ$ *vs.* ω, fig. 4 also shows the plots of $\eta(\dot\gamma)/\eta_\circ$ (open circles) *vs.* $\dot\gamma$ for the three samples and the fits to the Giesekus model. A comparison of the

values of $\eta_\circ$ obtained from the fits to the dynamic viscosity and shear viscosity data has been made in table 1. The fits to the shear viscosity data are found to work best at intermediate SiO_2 concentrations. Fig. 4 may be used to compare the degree of validity of the Cox-Merz condition for these samples. The Cox Merz rule is an empirical law for wormlike micelles which predicts $\eta(\dot{\gamma}) = |\eta^\star(\omega)|$ at $\omega = \dot{\gamma}$. We see that the agreement to the Cox-Merz rule is very poor for the pure CTAT sample (fig. 4 (a)) and improves for the intermediate (fig. 4 (b)) silica concentration, indicating the growth of giant wormlike micelles. We also measure the first normal force difference $N_1(\dot{\gamma})$ generated in each sample on the imposition of high shear rates and plot the results in Fig. 5. The magnitude of the normal stress difference is found to increase with SiO_2 concentration and indicates the formation of structures on the addition of SiO_2.

All the experiments and analyses discussed above are repeated for CTAT-SiO_2 mixtures with CTAT at concentrations of 1.4 wt.% (+ 0.178 mM of added NaOH added to increase the surface charge density of SiO_2), 1.95 wt.% and 2.6 wt.% respectively. The values of τ_R, $G_\circ$ and $\eta_\circ$ calculated by fitting the data to the models discussed above are plotted in Figs. 6-10. In fig. 6, we plot the results for CTAT 1.4wt.% + SiO_2. In fig. 7, we compare the values of τ_R, $G_\circ$ and $\eta_\circ$ for CTAT 1.4wt.% + SiO_2, without added NaOH (solid circles) and with 0.178mM NaOH (open triangles). All the plots for the mixtures with untreated SiO_2 show prominent peaks at SiO_2 weight percents between 1.3 and 1.9. The peaks clearly shift to lower SiO_2 concentrations when SiO_2 is treated

Table 1: The parameters α, $G_\circ$, τ_R and $\eta_\circ$, obtained by fitting the CTAT 1.4 wt.% + SiO_2 data to the models described above. α and $G_\circ$ are obtained from fits to the Cole Davidson model, the mean relaxation time τ_R is the inverse of the crossover frequency ${\omega_{co}}^{-1}$ and $\eta_\circ$ is obtained by fitting to the dynamic viscosity (DV) and the Giesekus (GM) models respectively.

SiO_2 wt.%	α	$G_\circ$	τ_R	$\eta_\circ$ Pa-s (DV)	$\eta_\circ$ Pa-s (GM)
0	-	1.3	1.54	2	1
0.85	~ 0.005	1.3	6.66	8	12
1.05	~ 0.01	1.5	9.09	12	18
1.3	0.01	1.8	11.11	18	21
1.95	0.2	2.1	8.77	19	20
2.6	0.3	1.9	5.40	11	12
3.9	0.6	1.8	3.57	7	8
5.2	0.7	1.1	2.00	2	2

with NaOH. Figs. 8 and 9 are the plots of τ_R, $G_\circ$ and $\eta_\circ$ for CTAT-silica mixtures with the CTAT weight percent fixed at 1.95 and 2.6 respectively. In table 1, we have compiled the values of the fitting parameters obtained from the fits to the frequency response and steady shear experiments on CTAT 1.4 wt.% as a function of added SiO_2 concentration. The values of $\eta_\circ$ obtained from fits to the dynamic viscosity and the Giesekus models are found to agree more at intermediate SiO_2 concentrations, indicating a better agreement with the empirical Cox-Merz rule under these conditions. In fig. 10, we have plotted $\eta_\circ$,

and τ_R for the different CTAT concentrations. For CTAT 1.4wt.%, the values of $\eta_\circ$, $G_\circ$ (not shown) and τ_R are found to peak at silica concentrations $\simeq$ CTAT concentrations. The peaks shift to lower SiO_2 concentrations for CTAT 1.95wt.%. For CTAT 2.6wt.%, the peaks disappear or possibly shift to very low silica concentrations that lie beyond the range of the present measurements.

5 Discussions

As discussed earlier, the stress relaxation in viscoelastic solutions of wormlike micelles is dominated by two processes, reptation and reversible scission [1, 16, 17]. The value of α in the Cole-Davidson model [15] gives an estimate of the width of the distribution of relaxation times. Multi-exponential relaxation processes are seen in dilute micellar solutions where $\alpha < 1$, with α increasing to 1 with increasing surfactant and/or salt concentrations [22, 23]. On adding SiO_2 to semi-dilute aqueous solutions of CTAT, we find a similar increase in the values of α suggesting an approach towards single exponential stress relaxation. From our viscosity data, it is clear that there is an increased tendency towards behavior characteristic of giant wormlike micelles, followed by significant departures on further addition of SiO_2 particles.

In this section, we explain the changes in the structure and dynamics of the cylindrical CTAT micelles when silica colloids are added to CTAT solutions under appropriate conditions. In the case of CTAT 1.4 wt.%, an addition of 1.3 wt.% SiO_2 particles results in the relaxation time increasing by 600%, $G_\circ$ in-

creasing by almost 37% and $\eta_\circ$ increasing by 1600% as compared to pure CTAT solutions. We find that the peaks in $\eta_\circ$ and τ_R shift to lower concentrations of SiO_2 as the surfactant concentration is increased from 1.4 to 1.95 wt.%, and disappear for CTAT 2.6wt.% (fig. 10). The increased fluidity of the samples on the addition of SiO_2 can be explained by considering the adsorption of the surfactant headgroups to the silica surfaces due to the attractive interactions between them [24]. The surfactants can be thought to form bilayers around the silica surface, with the headgroups constituting the outer layer and with the silica at the center. Enhanced formation of bilayers with increasing SiO_2 concentration can therefore explain the observed decreases in $\eta_\circ$, $G_\circ$ and τ_R. At lower SiO_2 concentrations, giant wormlike micelles outnumber the bilayers formed, and the presence of SiO_2 in solution serves to screen the electrostatic interaction between micelles, resulting in increased micellar entanglement, which manifests as peaks in plots of the relaxation times, shear moduli and viscosities of the samples. Addition of NaOH to 1.4wt.% CTAT results in a decrease in the magnitudes of $\eta_\circ$, $G_\circ$ and τ_R, with the peak shifting to lower SiO_2 concentrations (fig. 7). Treating the SiO_2 particles with NaOH increases their surface charge density by increasing the dissociation of the surface silanol groups. Increasing the surface charge on silica causes them to bind more strongly to the CTA^+, which results in the formation of bilayers at lower silica concentrations, clearly indicated by a shift in the peaks to the left (fig. 7). The dramatic changes in the intermicellar interactions on treating the SiO_2 particles with NaOH are thus responsible for

the observed changes in τ_R, $G_\circ$ and $\eta_\circ$. On continued addition of silica to the CTAT sample, a stage comes when all the headgroups get adsorbed onto the silica surfaces, leaving very few entangled micelles in solution.

Next, we focus on the shift in the viscosity peak to lower concentrations of added silica, when the surfactant concentration is increased to 1.95wt.% (fig. 8) and 2.6 wt.% (fig. 9). It is useful to mention here that these weight percents lie in the semi-dilute concentration regime of CTAT [25]. An increase in the surfactant concentration is known to result in an increase in the degree of ionization of the micelles [19]. Higher surfactant concentrations encourage the formation of bilayers at lower silica concentrations, resulting in the shifts of the peaks to lower silica concentrations. We conclude this section by stressing that we identify the peak as a signature of the formation of longer "worms" on the addition of SiO_2. We believe that this is followed by the formation of bilayers, resulting from the subsequent adsorption of the micellar headgroups to silica, which is manifested experimentally as a decrease in τ_R, $G_\circ$ and $\eta_\circ$.

6 Conclusions

In this paper, we study the modifications in the rheology of semi-dilute solutions of CTAT on the addition of submicrometer sized silica spheres. The drastic changes in rheology that we observe as a function of increasing silica concentration are explained by considering the electrostatic interactions between the surfactant and silica particles. We would like to note here that modifications

of the rheology of surfactant solutions by the controlled addition of particulate matter can have diverse uses in the industry.

References

[1] Rehage, H., Hoffmann H., Mol. Phys. 74 (1991) 933.

[2] Zapotocky, M., Ramos, L., Poulin, P., Lubensky, T. C., Weitz, D. A., Science 283 (1999) 209.

[3] Basappa, G., Suneel, Kumaran, V., Nott, P. R., Ramaswamy, S., Nayak, V. M., Rout, D., Eur. Phys. J. B 12 (1999) 269.

[4] Meeker, S. P., Poon, W. C. K., Crain, J, Terentjev, E. J., Phys. Rev. E 61 (2000) R6083.

[5] Koltover, I., Rädler, J. O., Safinya, C. R., Phys. Rev. Lett. 82 (1999) 1991.

[6] Rädler, J., Koltovich, I., Salditt, T., Safinya, C. R., Science 275 (1997) 810.

[7] Solomon, M. J., Saeki, T., Wan, M., Scales, P. J., Boger, D. V., Usui, H., Langmuir 15 (1999) 20.

[8] Adams, M., Dogic, Z., Keller, S. L., Fraden, S., Nature 393 (1998) 349.

[9] Krishnaswamy, R., Mitra, P., Raghunathan, V. A., Sood, A. K. Euro Phys Lett 62 (2003) 357.

[10] Menger, F. M., Eliseev, A. V., Langmuir 11 (1995) 1855.

[11] Hassan, P. A., Candau, S. J., Kern, F., Manohar, C., Langmuir 14 (1998) 6025.

[12] Iliopoulos, I., Wang, T. K., Audebert, R., Langmuir 7 (1991) 617.

[13] Chari, K., Antalek, B., Lin, M. Y., Sinha, S. K., J. Chem. Phys. 100 (1994) 5294.

[14] Yamanaka, J., Koga, T., Ise, N.; Hashimoto, T., Phys. Rev. E 53 (1996) R4314; Yamanaka, J., Hayashi, Y., Ise, N., Yamaguchi, T., Phys. Rev. E 55 (1997) 3028.

[15] Menon, N., Nagel, S. R., Venerus, D. C., Phys. Rev. Lett 73 (1994) 963.

[16] Cates, M. E., Candau, S. J., J. Phys. Condens. Matter 2 (1990) 5869.

[17] Cates, M. E., Macromol. 20 (1987) 2289; Cates, M. E., J. Phys. Chem. 94 (1990) 371.

[18] Granek, R and Cates, M. E., J. Chem. Phys. 96 (1992) 4758.

[19] Kern, F., Lequeux F., Zana, R., Candau, S. J. Langmuir 10 (1994) 1714.

[20] Fischer, P., Rehage, H., Rheol. Acta 36 (1997) 13.

[21] Giesekus, H., J. Non-Newt. Fluid Mech. 11 (1982) 69.

[22] Kern, F., Zana, R., Candau, S. J., Langmuir 7 (1991) 1344.

[23] Bandyopadhyay, R., Sood, A. K., Langmuir 19 (2003) 3121.

[24] Favoriti, P, Mannebach, M. H., Treiner, C., Langmuir 12 (1996) 4691.

[25] Soltero, J. F. A., Puig, J. E., Manero, O., Langmuir 12 (1996) 2654.

Figure 1: The elastic modulus $G'(\omega)$ and the viscous modulus $G''(\omega)$ *vs.* angular frequency ω for CTAT 1.4wt.%+SiO_2 samples. The solid lines show the fits to the real and imaginary parts of the Cole-Davidson model. The SiO_2 concentrations corresponding to each frequency response curve are (a) 0 wt.%, (b) 1.3wt.% and (c) 5.2wt.%.

Figure 2: Plot of the values of α *vs.* SiO_2 concentration for CTAT 1.4wt.% solutions. α is obtained by fitting the frequency response curves to the Cole-Davidson model.

Figure 3: Cole-Cole plots for CTAT 1.4 wt.% with SiO_2 concentrations 0 wt.% (open squares), 1.3 wt.% (plus-centered circles) and 5.2 wt.% (filled diamonds) respectively.

Figure 4: The normalized dynamic viscosity $\eta^\star(\omega)/\eta_\circ$ *vs.* ω (open squares) and the normalized shear viscosity $\eta(\dot\gamma)/\eta_\circ$ *vs.* shear rate (open circles) $\dot\gamma$ for CTAT 1.4wt.%+SiO_2 samples. The dashed lines show the fits of the dynamic viscosity to $\eta^\star = \frac{\eta_\circ}{\sqrt{1+\omega^2\tau_R^2}}$ and the solid lines show the fits to the Giesekus model. The SiO_2 concentration corresponding to each plot is (a) 0 wt.%, (b) 1.3wt.% and (c) 5.2wt.%.

Figure 5: The first normal stress difference N_1 *vs.* shear rate $\dot\gamma$ for CTAT 1.4wt.%+SiO_2 samples.

Figure 6: Plot of viscoelastic parameters for CTAT 1.4wt.%. (a) shows the calculation of the average relaxation time τ_R from the crossover frequency (cross-centred triangles), fits to the dynamic viscosity model (open circles) and the fits to the Giesekus model (solid circles) respectively. (b) shows the plots of the values of $G_\circ$ at different SiO_2 concentrations obtained from the fits to the Cole-Davidson model. (c) shows the values of $\eta_\circ$ obtained from the fits to the dynamic viscosity model (open diamonds) and the Giesekus model (solid circles).

Figure 7: Plots of the fitted parameters in the absence (filled circles) and in the presence (open triangles) of 0.178mM NaOH for CTAT 1.4wt.%. (a) and (b) show the calculation of the zero-shear viscosity $\eta_\circ$ from the fits to the Giesekus and the dynamic viscosity models respectively and (c) shows the plots of the values of $G_\circ$ at different SiO_2 concentrations obtained from the Cole-Davidson fits. (d) shows the values of τ_R obtained by using the relation $\tau_R \sim \omega_{co}^{-1}$.

Figure 8: Plots of the fitted parameters for CTAT 1.95wt.% + SiO_2. (a) shows the plot of the average relaxation time τ_R obtained from the inverse of the crossover frequency (solid triangles), fits to the dynamic viscosity model (open diamonds) and the fits to the Giesekus model (solid circles). (b) shows the plots of the values of $G_\circ$ at different SiO_2 concentrations obtained from the Cole-Davidson fits and (c) shows the values of $\eta_\circ$ obtained from the fits to the functional form suggested for $\eta^\star$ (open diamonds) and the Giesekus model (filled circles).

Figure 9: Plots of the fitted parameters for CTAT 2.6wt.% + SiO_2. (a) shows the plot of the average relaxation time τ_R i) obtained using the relation $\tau_R = \omega_{co}^{-1}$ (solid triangles), ii) from fits to the dynamic viscosity model (open diamonds) and (iii) from the fits to the Giesekus model (solid circles), (b) shows a plot of the values of $G_\circ$ at different SiO_2 concentrations, obtained from the Cole-Davidson fits and (c) shows the values of $\eta_\circ$ obtained from the fits to the dynamic viscosity model (open diamonds) and the Giesekus model (solid circles).

Figure 10: Plot of the zero-shear viscosity $\eta_\circ$ obtained by fitting to the dynamic viscosity data for of 1.4wt.% (circles), 1.95wt.% (up-triangles) and 2.6wt.% (down-triangles) CTAT. The relaxation times τ_R obtained from ω_{co} are also plotted *vs.* silica concentration for the three concentrations of CTAT and are indicated by the same symbols described above. The dotted lines are guides to the eye.

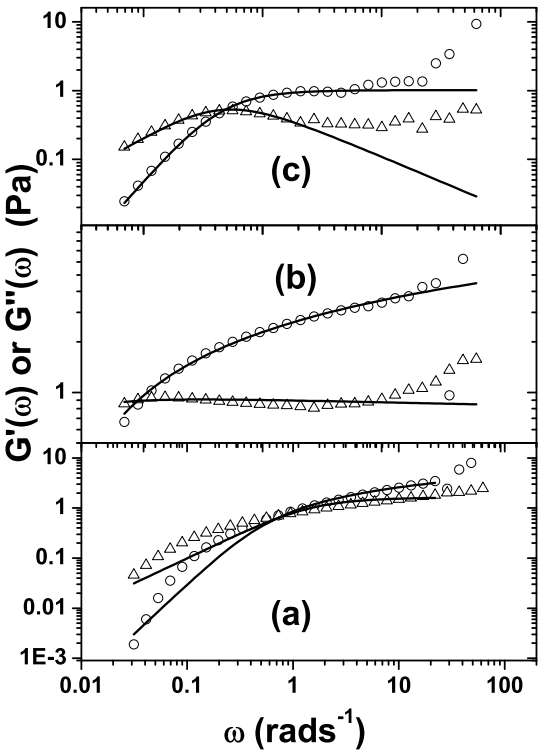
G'(ω) or G''(ω) (Pa)
10
1
0.1
(c)
1
(b)
10
1
0.1
0.01
1E-3
(a)
0.01
0.1
1
10
100
ω (rads-1)

This figure "rbfig2.PNG" is available in "PNG" format from:

http://arXiv.org/ps/cond-mat/0409435v1

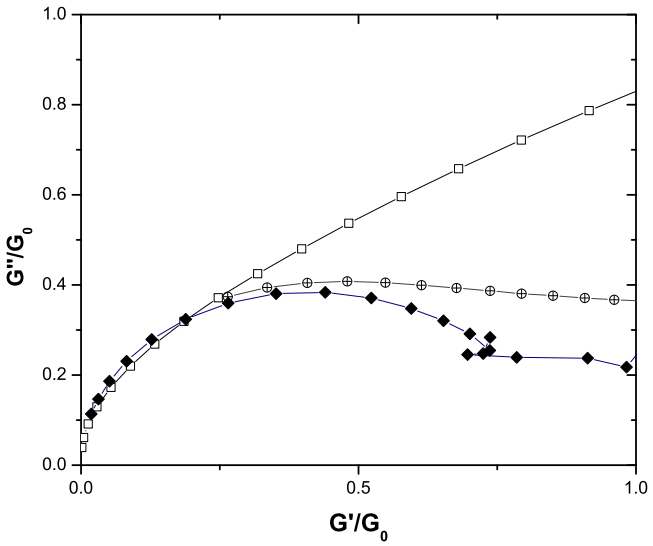
1.0
0.8
0.6
0.4
0.2
0.0
G''/G0
0.0
0.5
1.0
G'/G0

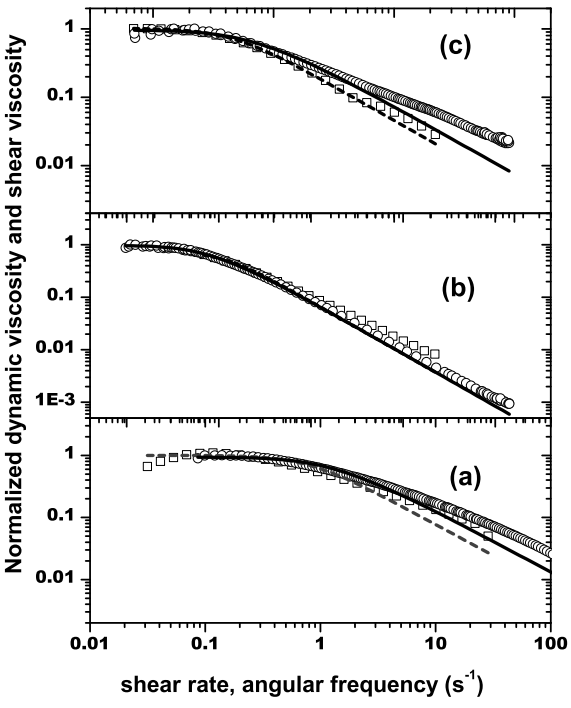
Normalized dynamic viscosity and shear viscosity
shear rate, angular frequency (s-1)
(c)
(b)
(a)
1
0.1
0.01
1E-3
0.01
0.1
1
10
100

This figure "rbfig5.PNG" is available in "PNG" format from:

http://arXiv.org/ps/cond-mat/0409435v1

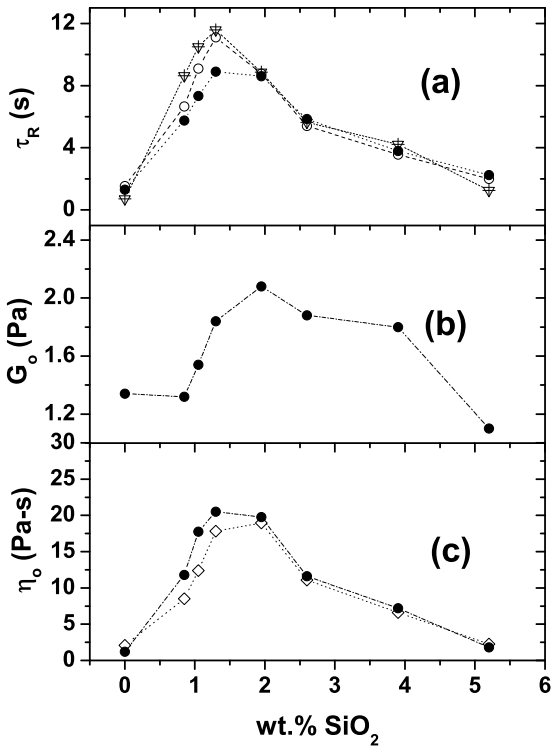
12
8
4
0
τ_R (s)
(a)
2.4
2.0
1.6
1.2
G_o (Pa)
(b)
30
25
20
15
10
5
0
η_o (Pa-s)
(c)
0
1
2
3
4
5
6
wt.% SiO_2

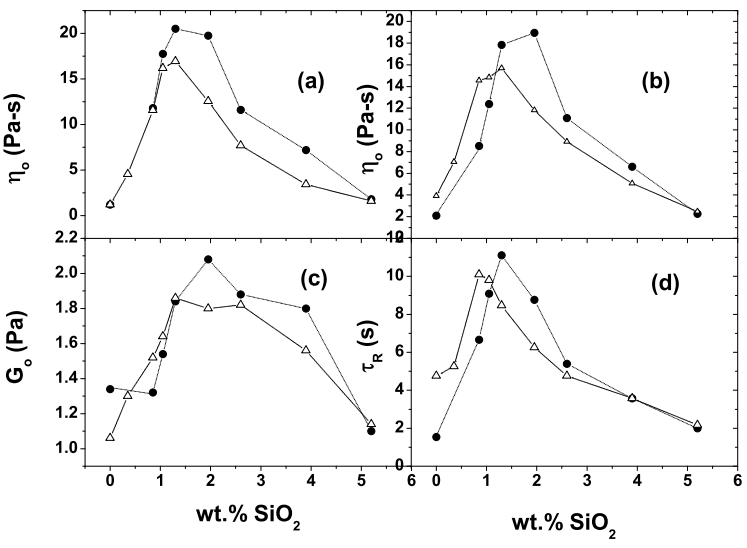
(a)
(b)
(c)
(d)
η_o (Pa-s)
η_o (Pa-s)
G_o (Pa)
τ_R (s)
wt.% SiO_2
wt.% SiO_2

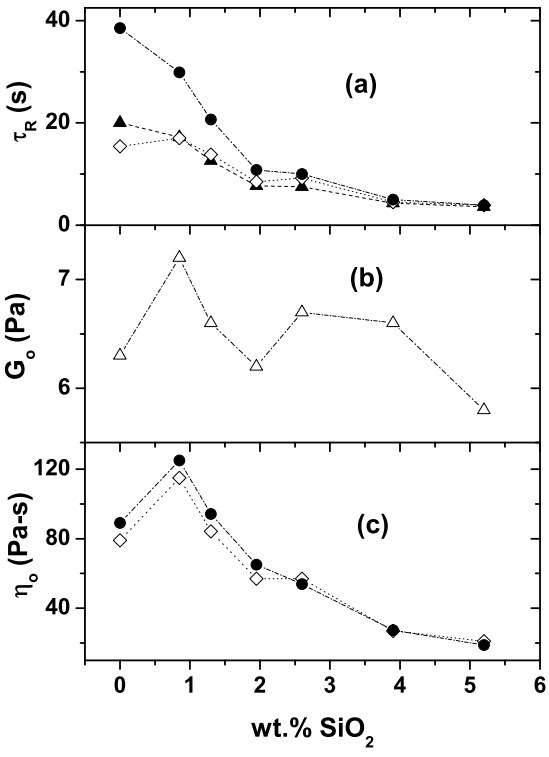
40
20
0
τ_R (s)
(a)
7
6
G_o (Pa)
(b)
120
80
40
η_o (Pa-s)
(c)
0
1
2
3
4
5
6
wt.% SiO_2

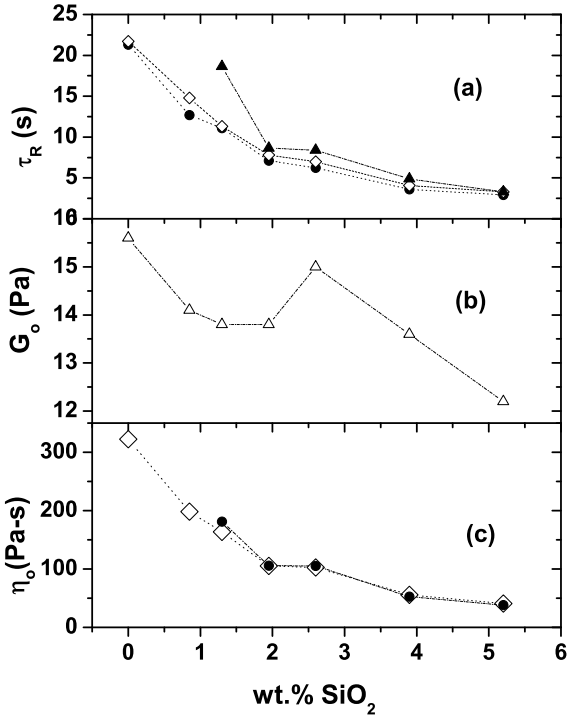
25
20
15
10
5
τ_R (s)
(a)
16
15
14
13
12
G_o (Pa)
(b)
300
200
100
0
η_o(Pa-s)
(c)
0
1
2
3
4
5
6
wt.% SiO_2

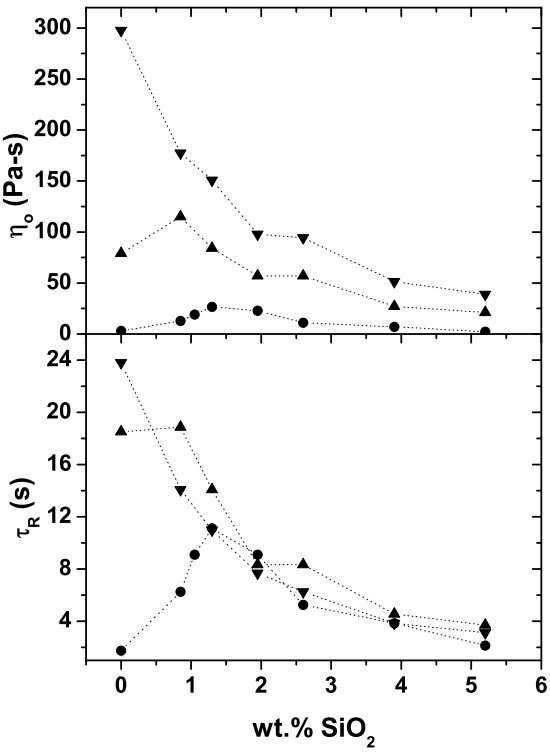
300
250
200
150
100
50
0
η_o (Pa-s)
24
20
16
12
8
4
τ_R (s)
0
1
2
3
4
5
6
wt.% SiO_2